# Density Functional Theory and Time-Resolved Resonance Raman Investigation of the Photocyclization of 2-Pyridyl Phenyl Ketone in Acid Solution†

**Xiangguo Guan, Yong Du, Jiadan Xue, and David Lee Phillips***

*Department of Chemistry, The University of Hong Kong, Pokfulam Road, Hong Kong, P. R. China*

*Received: September 25, 2008; Revised Manuscript Received: December 18, 2008*

Density functional theory computations and nanosecond time-resolved resonance Raman (ns-TR$^3$) spectroscopy experiments were done to study the photocyclization of 2-pyridyl phenyl ketone in acid solution. The most probable cyclization pathway was assigned to the reaction RX1, which had the lowest free-energy barrier. The factors that determine the free-energy barriers among the different reactions examined were discussed. Solvent effects on these reactions were also explored by calculations that included a polarizable continuum model for the bulk solvent effect.

## Introduction

The photophysics and photochemistry of benzophenone have been extensively studied in order to better understand its fast intersystem crossing (ISC) and lowest triplet electronic excited-states hydrogen abstraction reactions with other molecules.[1,2] Pyridyl phenyl ketones (denoted hereafter by *S*-PPK, where *S* is the number representing the different position of the N atom on the aromatic rings) are a type of benzophenone derivative and have also been investigated to better understand the properties of their (n−$\pi$*, $\pi$−$\pi$*) singlet and triplet states due to the influence of the N atom in the aromatic ring.[3−5] 2-Pyridyl phenyl ketone (2-PPK) in particular has received additional attention due to its unusually short triplet lifetime compared to those of 3-PPK and 4-PPK, which are able to abstract a hydrogen atom from a donor or solvent in the excited state in a manner like the triplet state of benzopheone.[3,5,6] Photocyclization of the triplet 2-PPK is thought to be the main process that could lead to its unusually short triplet lifetime.[4,5,7] Two likely possibilities have been proposed for the cyclization process.[4,5,7] The first possibility was a cyclization reaction involving attack of a nitrogen atom.[7] The second possibility was that the major transient species observed in some time-resolved experiments was formed from a reaction involving an attack of the carbon atom.[4,5] This uncertainty in which the cyclization process occurs and an unclear identity of the major transient species prompted us to use density functional theory (DFT) calculations to discern the most likely reaction pathway and nanosecond time-resolved resonance Raman (ns-TR$^3$) experiments to characterize and clearly confirm the identity of the major transient species observed on the nanosecond to microsecond time scales. Density functional theory (DFT) methods have been demonstrated to perform well for finding the geometry, zero-point vibrational energies, and reaction barriers for a number of radical reactions.[8−11] Time-resolved resonance Raman (ns-TR$^3$) has been widely used to unambiguously characterize and identify transient species and learn more about their structural and electronic properties.[12−15] In this paper, we systematically compare the barriers of eight cyclization pathways for the 2-PKK molecules (see Scheme 1) in order to find the most favorable pathway predicted from the DFT calculations. We also performed the first nanosecond time-resolved resonance Raman (ns-TR$^3$) spectroscopic characterization of the transient species observed on the nanosecond to microsecond time scales in an acid solution. The results from these calculations and experiments consistently indicate the cyclization process involves an attack of the nitrogen atom of 2-PPK.

## Computational and Experimental Methods

All of reactant, product, and transition-state geometries involved in the reactions studied were optimized at the UB3LYP/6-31G* level of theory using the Gaussian 03 program suite.[16] Vibrational frequency calculations were performed for all of the stationary points in order to obtain corrections for the zero-point energies (ZPEs) and make sure that the computed transition states were first-order saddle points. The ZPE correction and free energies used the entropies calculated within Gaussian and were added to the single-point energies (UB3LYP/6-31G*//UB3LYP/6-31G*). Intrinsic reaction coordination (IRC) computations were done to confirm that the transition states connected the corresponding reactants and products. Solvent effects were also considered by UB3LYP/6-31G* optimizations of the gas-phase stationary points using a simple SCRF method based on a polarizable continuum model (PCM).[17] A higher basis set, 6-311G**, was used in the DFT calculations employed to obtain the calculated Raman frequencies that were compared with experimental results in order to make vibrational assignments.

Samples of 2-benzoylpyridine were obtained commercially from Aldrich (>99% purity). Spectroscopic-grade MeCN and deionized water were used as solvents for preparing the samples used in the experiments presented in this work. The nanosecond time-resolved resonance Raman (ns-TR$^3$) measurements were done using an experimental apparatus described previously.[12−15,18] The pump wavelength was 266 nm supplied by the fourth harmonic of a Spectra Physics Laboratory 170-10 Nd:YAG Q-switched laser, and the 354.7 nm probe wavelength came from the third harmonic from the second Nd:YAG laser (Spectra Physics GCR-150-10). The time delay between the pump and probe beam was controlled electronically by a pulse delay generator and monitored by a photodiode and a 500 MHz oscilloscope. The time resolution of the TR$^3$ experiments was ∼10 ns. The energy of the pump and probe pulses used in the experiments was in the 2.5−3.5 mJ range. A near collinear

† Part of the "Max Wolfsberg Festschrift".

* To whom correspondence should be addressed. E-mail: phillips@hkucc.hku.hk

10.1021/jp808532n CCC: $40.75 
Published on Web 01/26/2009

**SCHEME 1**

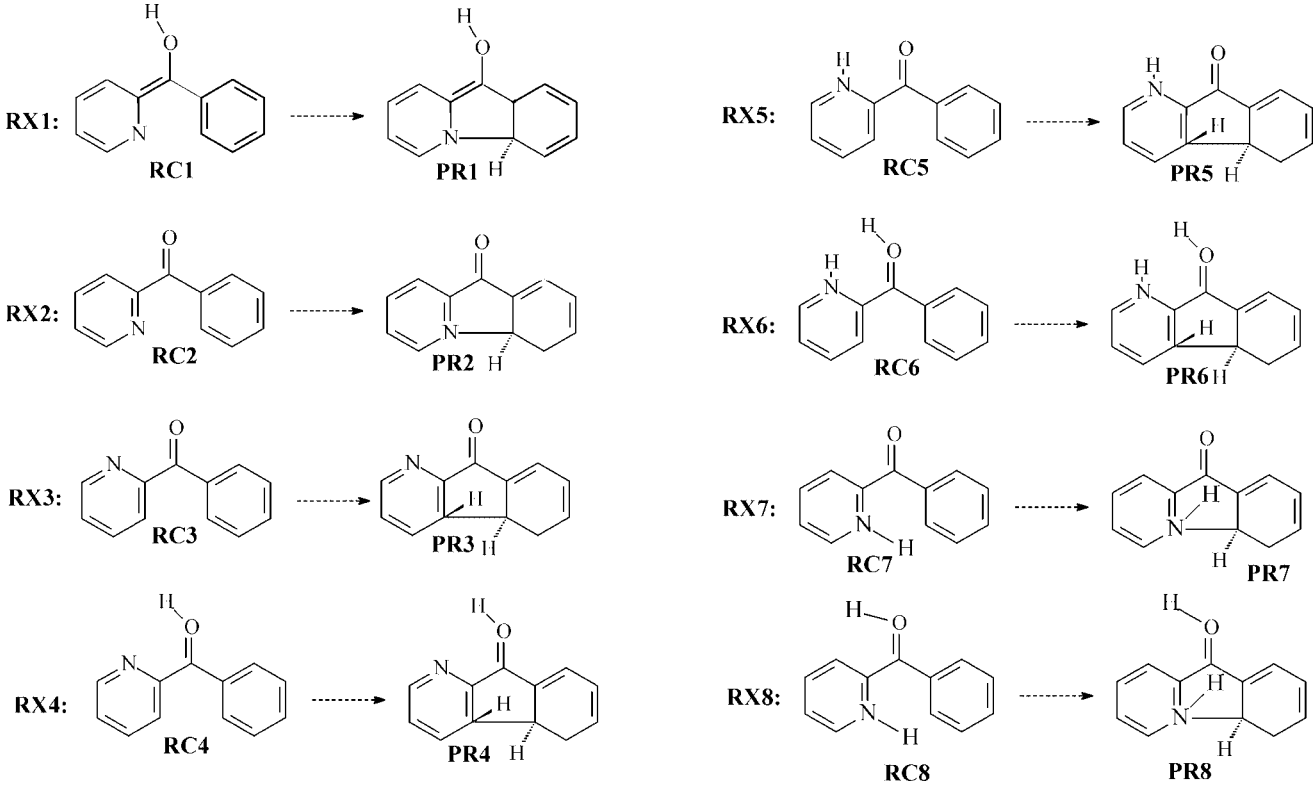


geometry was used to focus the pump and probe beam onto a flowing liquid stream of sample. The Raman scattering was collected in a backscattering geometry and detected by a liquid-nitrogen-cooled CCD detector for 30−60 s before being read out to an interfaced PC computer. Approximately 10−20 of these readouts were accumulated to get a resonance Raman spectrum. The spectra presented in this work were obtained from subtraction of an appropriately scaled probe-before-pump spectrum from the corresponding pump−probe spectrum. Acetonitrile Raman bands were used to calibrate the TR[3] spectra with an estimated accuracy of ±5 $cm^{-1}$ in absolute frequency.

## Results and Discussion

Scheme 1 shows eight possible cyclization reactions of 2-pyridyl ketone in its triplet state. These reactions can be categorized into two basic types, namely, a lone pair involved kind of reaction or a nonlone pair involved kind of reaction. The lone pair involved reactions include reactions RX1 and RX2, which have a center nitrogen atom. The nonlone pair involved reactions include reactions RX3−RX8. Although RX7 and RX8 also contain a center nitrogen atom, the lone pair electrons disappear through formation of an O−H bond. Figure 1 show a schematic diagram of the gas-phase calculated free-energy barriers found for the cyclization reactions examined here (solvent effects on the reactions will be discussed in a subsequent section). Inspection of Figure 1 shows that the lone pair involved reactions (reactions RX1 and RX2) have relatively lower free-energy barriers and are both exothermic. It is worth noting that the RX1 reaction has the lowest activation free-energy barrier and the most negative exothermic energy. This indicates that reaction RX1 is both kinetically and thermodynamically the most favorable one. This most feasible reaction pathway (RX1) agrees with one of the mechanisms proposed previously.[7] The calculated free energies have uncertainties of several kcal/mol, but the large differences in the estimated barriers to reactions for RX1 compared to the other reactions considered indicates this uncertainty will not affect the conclusion that RX1 is the most feasible of the reactions considered. To explain the energy barrier differences of the lone pair involved reactions and the nonlone pair involved reactions, reactions RX1 and RX3 were used as representative reactions (see Figure 2). In reaction RX3 the p orbital in the center atom C1 needs to flip nearly 90° from the reactant RC3 to transition state TS3, while in reaction RX1 the lone pair orbital in the center atom N1 undergoes very little change from the reactant RC1 to the transition state TS1, which suggests less energy is needed to overcome the barrier to reaction in the lone pair involved reaction than in the nonlone pair involved reaction. NBO analysis was done to help examine the internal barrier differences of the two lone pair involved reactions RX1 and RX2. For the RX2 reaction the charge distribution on the

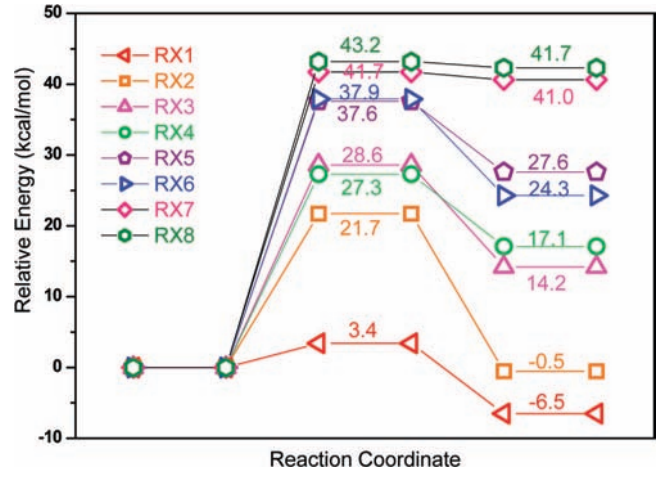


**Figure 1.** Free-energy diagram of the cyclization reactions examined here.

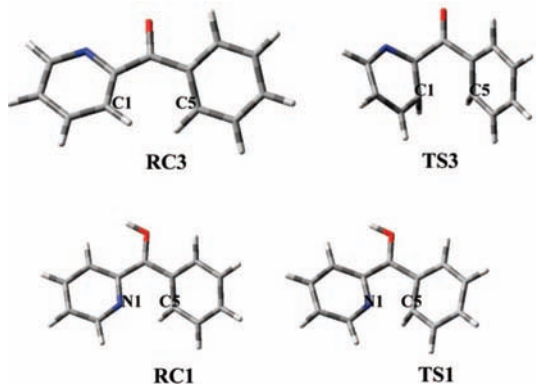


**Figure 2.** Schematic diagrams of the optimized geometry of RC1, TS1 and RC3, TS3.

**TABLE 1: Key Structural Changes of the Six Cyclization Reactions**[a]

| Cyclization Reactions | RC | TS | PR |
|---|---|---|---|
| RX1 | 2.515 ($N_1$-$C_5$) | 2.000 ($N_1$-$C_5$) | 1.502 ($N_1$-$C_5$) |
| RX2 | 2.990 ($N_1$-$C_5$) | 2.015 ($N_1$-$C_5$) | 1.484 ($N_1$-$C_5$) |
| RX3 | 3.303 ($C_1$-$C_5$) | 2.214 ($C_1$-$C_5$) | 1.582 ($C_1$-$C_5$) |
| RX4 | 3.267 ($C_1$-$C_5$) | 2.112 ($C_1$-$C_5$) | 1.593 ($C_1$-$C_5$) |
| RX5 | 3.382 ($C_1$-$C_5$) | 2.114 ($C_1$-$C_5$) | 1.589 ($C_1$-$C_5$) |
| RX6 | 3.272 ($C_1$-$C_5$) | 2.054 ($C_1$-$C_5$) | 1.594 ($C_1$-$C_5$) |
| RX7 | 3.277 ($C_1$-$C_5$) | 1.845 ($C_1$-$C_5$) | 1.633 ($C_1$-$C_5$) |
| RX8 | 3.222 ($C_1$-$C_5$) | 1.804 ($C_1$-$C_5$) | 1.615 ($C_1$-$C_5$) |

[a] Note: RC = reactant complex, TS = transition state, PR = product.

nitrogen atom changes from −0.46 in RC2 to −0.35 in TS2, while for the RX1 reaction the charge distribution on the nitrogen atom changes very little from −0.31 in RC1 to −0.32 in TS1. Thus, the ability of delocalizing the negative charges on the nitrogen atom appear to be correlated with or help determine the activation free-energy barriers of the lone pair involved reactions.

It is also interesting to compare the changes in the geometry with the activation free-energy barriers. Table 1 shows the key geometry information obtained at the UB3LYP/6-31G* level of theory for the RC (reactant), TS (transition state), and PR (product) of the cyclization reactions examined here. For example, in reaction RX1 as the reaction goes from the reactant complex to the transition state R15 (the distance between the N1 and C5 atoms) changes substantially from 2.515 to 2.0 Å. As the reaction goes from the transition state to the product the N−C bond is completely formed with a bond length of 1.502 Å in the product. The lone pair involved reactions, RX1 and RX2, have a lower R15 value, 2.515 and 2.990 Å, while the other six nonlone pair involved cyclization reactions, regardless of their different charges and protons, all have noticeably larger R15 values of about 3.3 Å.

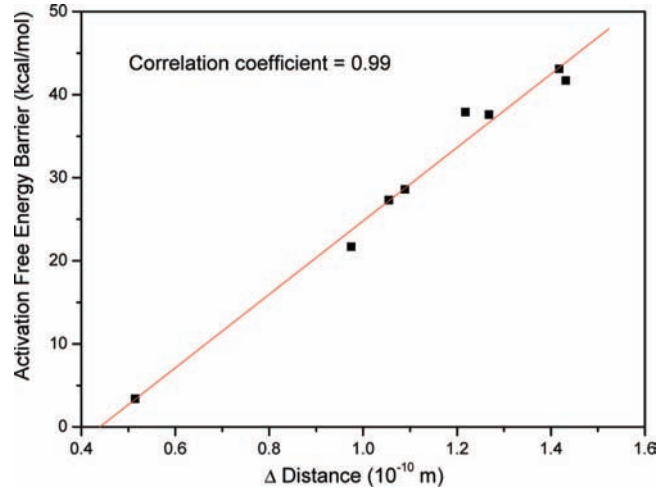


**Figure 3.** Correlation between the Δdistance and the activation free-energy barriers for reactions RX1−RX8 (see text for details).

**TABLE 2: Calculated Activation Free Energies ($\Delta G^{\ddagger}$, kcal/mol) at 298 K for Reactions RX1−RX8 in Vacuum and Selected Solvents (see text for details)**

| RXs | $\Delta G^{\ddagger}$ (Vacuum) | $\Delta G^{\ddagger}(C_6H_{12})$, $\varepsilon = 2.0$ | $\Delta G^{\ddagger}$(THF), $\varepsilon = 7.58$ | $\Delta G^{\ddagger}$(ACN), $\varepsilon = 36.64$ | $\Delta G^{\ddagger}(H_2O)$ $\varepsilon = 78.39$ |
|---|---|---|---|---|---|
| RX1 | 3.4 | 1.3 | 0.7 | 0.46 | 0.2 |
| RX2 | 21.7 | 11.7 | 9.3 | 8.2 | 8.1 |
| RX3 | 28.6 | 31.0 | 28.5 | 27.3 | 27.2 |
| RX4 | 27.3 | 25.1 | 23.0 | 22.0 | 21.7 |
| RX5 | 37.6 | 32.5 | 29.3 | 28.3 | 27.9 |
| RX6 | 37.9 | 35.3 | 32.3 | 31.4 | 31.2 |
| RX7 | 41.7 | 37.6 | 33.6 | 32.1 | 32.1 |
| RX8 | 43.1 | 36.5 | 32.9 | 31.4 | 31.4 |

The correlation of the activation free-energy barrier with the changes of the distance (Δdistance) from the reactant complex to the transition state (Δdistance = $R15_{reactant} - R15_{transition\ state}$) is shown in Figure 3. The correlation coefficient is as high as 0.99, which indicates there is a very strong correlation between the activation free-energy barrier and the geometry changes associated with the distance (Δdistance) from the reactant complex to the transition state (Δdistance = $R15_{reactant}$ − R15transition state). The slope of the correlation is positive and indicates that a smaller distance change during the reaction should result in a lower activation free-energy barrier.

We note that previously reported experiments for the photocyclization reaction of 2-PPK were performed in the solution phase, and hence, solvent effects could noticeably influence the activation barriers. Thus, we considered solvent effects on these reactions. The solvent effects on these reactions were investigated using the UB3LYP/6-31G* optimizations of the gas-phase stationary points and then using the SCRF method based on a polarizable continuum model (PCM) developed by Tomasi and co-workers.15 We did the calculations in solvents ranging from a nonpolar cyclohexane

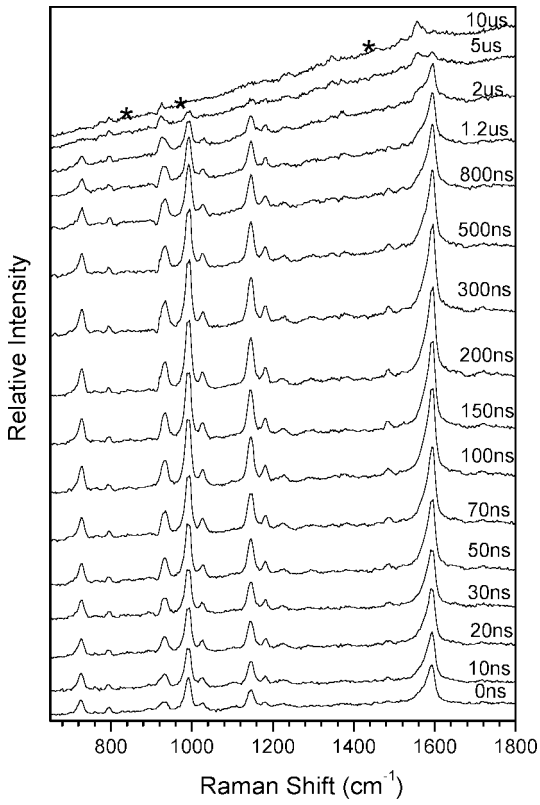


**Figure 4.** $TR^3$ spectra of 1.5 mM 2-PPK with pH = 1 and 266 nm pump and 354.7 nm probe wavelengths. The asterisk (*) marks subtraction artifacts.

solvent with a dielectric constant of $\varepsilon = 2.0$ to the highly polar water solvent with the highest dielectric constant considered of $\varepsilon = 78.39$. The results of these calculations are shown in Table 2 and suggest that the solvent effects have a noticeable impact on the cyclization reactions. As the dielectric constant gradually increases the activation free-energy barrier decreases gradually. Comparison of the dipole moment between the reactant complex and the relevant transition state shows that all of the transition states have a higher polarity than their corresponding reactant complex. Thus, the solvated energy is higher in the transition state than that of the reactant complex, which decreases the activation barrier of the corresponding reaction in the solvent. We note that the results in both the gas and solution phases predict that the RX1 cyclization is the most favorable one by a substantial degree compared to the other cyclization reactions considered.

From the results of the preceding theoretical calculations we found that the most feasible reaction pathway appears to be RX1, which has a protonated carbonyl moiety. Next, we did some ns-$TR^3$ experiments in acid solution to learn more about the transient species previously observed in time-resolved transient absorption experiments reported in the literature.[4,5] Figure 4 displays representative ns-$TR^3$ spectra of 2-PPK in an acid pH = 1, 1:1 $H_2O$:MeCN solution acquired with various time delays between the pump and probe pulses that are indicated next to the spectra. Inspection of Figure 4 shows there is a clear transient species observed over the nanosecond to microsecond time scale that then decays completely on the microsecond time scale. This is consistent with the previously reported time-resolved transient absorption results.[4,5] The species observed in the ns-$TR^3$ spectra of Figure 4 that has characteristic Raman bands at 721, 990, 1142, and 1594 $cm^{-1}$ was assigned to PR1, which is directly produced from the triplet state of 2-PPK species through reaction pathway RX1. The assignment of the transient species was based on a comparison of

**SCHEME 2: Proposed Cyclization Reaction Pathway for 2-Pyridyl Phenyl Ketone (2PPK; see text for details)**

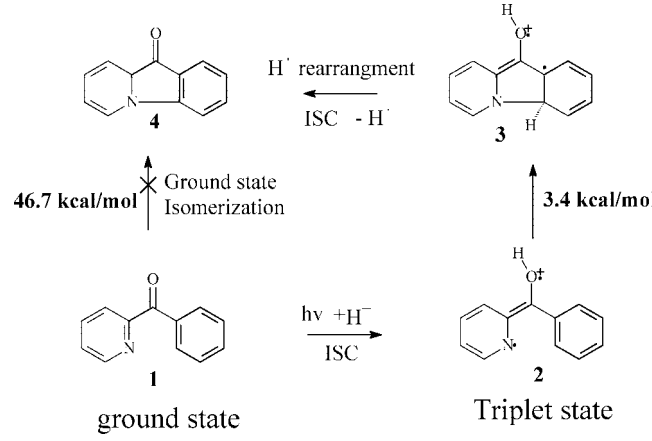


the $TR^3$ experimental vibrational frequencies to those calculated from the DFT calculations for four probable species [e.g., the ground state of 2-PPK, the carbonyl protonated triplet 2-PPK species, the PR1 species, and the cyclization product of 2-PPK (denoted **1**, **2**, **3**, and **4**, respectively, in Scheme 2)]. Figure 1S, Supporting Information, displays a comparison of the 70 ns $TR^3$ spectrum from Figure 4 (e.g., spectrum B in Figure 1S, Supporting Information) to those predicted from the DFT calculations for the ground state of 2-PPK, the carbonyl protonated triplet 2-PPK species, the PR1 species, and the cyclization product of 2-PPK [spectra C, D, A, and E, respectively, in Figure 1S, Supporting Information]. The strongest predicted Raman band at 1413 $cm^{-1}$ and another strong band >1600 $cm^{-1}$ of the ground state of 2-PPK (spectrum C) in Figure 1S, Supporting Information, do not appear in the experimental $TR^3$ spectrum B, and this appears to rule out an assignment to the ground state of 2-PPK. Similarly, there are several predicted strong Raman bands above 1600 $cm^{-1}$ in spectrum E in Figure 1S, Supporting Information, for the cyclization product of 2-PPK that do not appear in the experimental $TR^3$ spectrum B, and this appears to rule out an assignment to this species. There are strong predicted Raman bands in the 840−900 $cm^{-1}$ region and the 1280−1440 $cm^{-1}$ region for spectrum D in Figure 1S, Supporting Information, for the carbonyl protonated triplet 2-PPK species that do not appear in the experimental $TR^3$ spectrum B, and this appears to rule out an assignment to this species. However, the vibrational frequencies predicted from the DFT calculations for the PR1 species (spectrum A in Figure 1S, Supporting Information) appear to have a reasonable correlation to the experimental $TR^3$ spectrum B. Table 1S in the Supporting Information compares the experimental Raman band vibrational frequencies for the 70 ns $TR^3$ spectrum from Figure 4 to those predicted from the DFT calculations for the PR1 species in Figure 1S, Supporting Information. Inspection of Table 1S, Supporting Information, reveals there is reasonable agreement between the experimental and calculated vibrational frequencies with the calculated vibrational frequencies being within about 8.5 $cm^{-1}$ on average for the 10 experimental Raman band frequencies compared to the calculated ones. Examination of the experimental $TR^3$ spectrum to the calculated PR1 spectrum also shows reasonable agreement with the calculated normal Raman spectrum of the PR1 species with differences in the relative intensities that can be accounted for by the fact that the experimental spectrum is resonantly enhanced while the calculated spectrum is for a normal Raman spectrum. These results suggest the species observed in the $TR^3$ spectra is likely the PR1 species. Table 2S in the Supporting Information lists selected results from TD-DFT calcula-

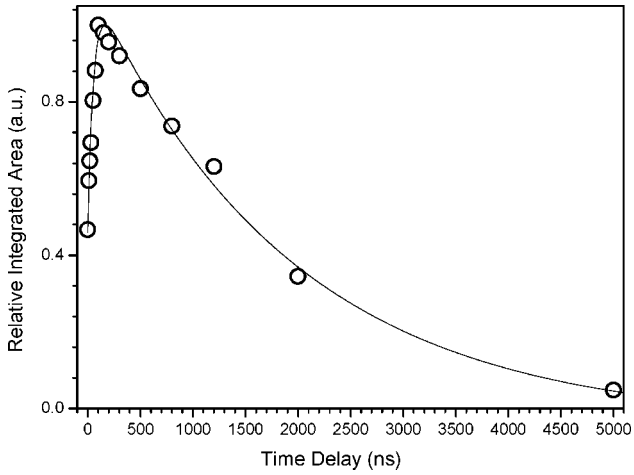


**Figure 5.** Dynamics of the transient species observed in acid aqueous solution (open circles) and fit with a two-exponential function with a ~54 ns growth time constant and a 1850 ns decay time constant. The data displayed here were derived from the $TR^3$ spectra shown in Figure 4.

tions for the electronic transitions and their oscillator strengths in the 250−500 nm region. The TD-DFT calculations predict the PR1 species has strong electronic transitions at about 286 and 432 nm, and this is consistent with the transient absorption experiments for 2-PPK in aqueous solution that observed strong broad transient absorption over the 300−480 nm region.[4,5]

Figure 5 displays the dynamics of the transient species using the integrated areas of the 1594 $cm^{-1}$ Raman band observed in the $TR^3$ spectra in Figure 4. The data points can be well fit by a two-exponential function with a growth time constant of 54 ns and a decay time constant of 480 ns. Through a simple conversion using transition-state theory the experimental growth time constant of 54 ns is equivalent to an activation free-energy barrier of about 6 kcal/mol, which is in reasonable agreement with the low free-energy barriers of RX1 (in the 0.2−3.4 kcal/mol range, see Scheme 1 and Table 2). The decay time constant of 1850 ns is in agreement with that of the triplet diradical species measured for the transient absorption spectra in water that had a time constant of 2 $\mu$s in the literature.[4] On the basis of the theoretical and experimental results presented here we propose a cyclization reaction mechanism for 2-PPK in acid solution that is shown in Scheme 2. Direct excitation of the ground state 2-PPK **1** in an acid solution will lead after ISC from a singlet excited state to formation of the triplet state species **2**, then this triplet species **2** undergoes a cyclization reaction to form the triplet transient intermediate **3**, and then, finally, the cyclic triplet transient intermediate **3** undergoes ISC and proton release to produce the final product **4**. This proposed reaction mechanism is consistent with our present results and some results reported in the literature.[7] We also performed a ground-state reaction pathway calculation and found the ground-state cyclization reaction is highly unlikely because its free-energy barrier is as high as 46.7 kcal/mol. It is the excited state that activates the reactant and makes the cyclization reaction feasible.

## Conclusions

We reported density functional theory (DFT) computations for the photocyclization of 2-pyridyl phenyl ketone (2-PPK) in acid solution. The most probable cyclization pathway was assigned to the reaction with the lowest free-energy barrier. The lone pair electrons and charge distributions are thought to be the key factors in determining the free-energy barrier of the cyclization reactions investigated here. The calculated free-energy barrier of the most probable cyclization reaction is consistent with available experimental data. Solvent effects on these reactions were also explored by calculations that included a polarizable continuum model of the bulk solvent. Nanosecond time-resolved resonance Raman (ns-$TR^3$) spectroscopy experiments were done to further confirm the assignment of the transient species observed on the nanosecond to microsecond time scales.

**Acknowledgment.** This research has been supported by grants from the Research Grants Council of Hong Kong (HKU-7039/07P) to D.L.P. D.L.P. thanks the Croucher Foundation for the award of a Croucher Foundation Senior Research Fellowship (2006−07) and the University of Hong Kong for an Outstanding Researcher Award (2006).

**Supporting Information Available:** Cartesian coordinates, total energies for the stationary points investigated, Table 1S shows a comparison of the vibrational frequencies of the 70 ns $TR^3$ spectrum of Figure 4 to the vibrational frequencies calculated for the PR1 species, and Figure 1S shows a comparison of the $t = 70$ ns $TR^3$ spectrum in Figure 4 to the DFT-calculated normal Raman spectrum of the PR1 species. This material is available free of charge via the Internet at http://pubs.acs.org.

## References and Notes

(1) Gilmore, E. H.; Gibson, G. E.; McClure, D. S. *J. Chem. Phys.* **1952**, *20*, 829–836.
(2) Turro, N. J. *Modern Molecular Photochemistry*; University Science Books: Mill Valley, CA, 1991.
(3) Ortica, F.; Elisei, F.; Favaro, G. *J. Chem. Soc., Faraday Trans.* **1995**, *91*, 3405–3413.
(4) Bortolus, P.; Elisei, F.; Favaro, G.; Monti, S.; Ortica, F. *J. Chem. Soc., Faraday Trans.* **1996**, *92*, 1841–1851.
(5) Ortica, F.; Elisei, F.; Favaro, G. *J. Phys. Org. Chem.* **1999**, *12*, 31–38.
(6) Favaro, G. *J. Chem. Soc., Perkin Trans. 2* **1976**, 869–876.
(7) Hurt, C. R.; Filipesc, N. *J. Am. Chem. Soc.* **1972**, *94*, 3649–3651.
(8) Fischer, H.; Radom, L. *Angew. Chem., Int. Ed.* **2001**, *40*, 1340–1371.
(9) Fox, T.; Kollman, P. A. *J. Phys. Chem.* **1996**, *100*, 2950–2956.
(10) Guan, X. G.; Phillips, D. L.; Yang, D. *J. Org. Chem.* **2006**, *71*, 1984–1988.
(11) Smith, D. M.; Nicolaides, A.; Golding, B. T.; Radom, L. *J. Am. Chem. Soc.* **1998**, *120*, 10223–10233.
(12) Chan, P. Y.; Kwok, W. M.; Lam, S. K.; Chiu, P.; Phillips, D. L. *J. Am. Chem. Soc.* **2005**, *127*, 8246–8247.
(13) Ma, C.; Du, Y.; Kwok, W. M.; Phillips, D. L. *Chem. Eur. J.* **2007**, *13*, 2290–2305.
(14) Du, Y.; Ma, C. S.; Kwok, W. M.; Xue, J. D.; Phillips, D. L. *J. Org. Chem.* **2007**, *72*, 7148–7156.
(15) Du, Y.; Xue, J. D.; Ma, C. S.; Kwok, W. M.; Phillips, D. L. *J. Raman Spectrosc.* **2008**, *39*, 503–514.
(16) Frisch, M. J.; Trucks, G. W.; Schlegel, H. B.; Scuseria, G. E.; Robb, M. A.; Cheeseman, J. R.; Montgomery, J. A., Jr.; T. V.; Kudin, K. N.; Burant, J. C.; Millam, J. M.; Iyengar, S. S.; Tomasi, J.; Barone, V.; Mennucci, B.; Cossi, M.; Scalmani, G.; Rega, N.; Petersson, G. A.; Nakatsuji, H.; Hada, M.; Ehara, M.; Toyota, K.; Fukuda, R.; Hasegawa, J.; Ishida, M.; Nakajima, T.; Honda, Y.; Kitao, O.; Nakai, H.; Klene, M.; Li, X.; Knox, J. E.; Hratchian, H. P.; Cross, J. B.; Bakken, V.; Adamo, C.; Jaramillo, J.; Gomperts, R.; Stratmann, R. E.; Yazyev, O.; Austin, A. J.; Cammi, R.; Pomelli, C.; Ochterski, J. W.; Ayala, P. Y.; Morokuma, K.; Voth, G. A.; Salvador, P.; Dannenberg, J. J.; Zakrzewski, V. G.; Dapprich, S.; Daniels, A. D.; Strain, M. C.; Farkas, O.; Malick, D. K.; Rabuck, A. D.; Raghavachari, K.; Foresman, J. B.; Ortiz, J. V.; Cui, Q.; Baboul, A. G.; Clifford, S.; Cioslowski, J.; Stefanov, B. B.; Liu, G.; Liashenko, A.; Piskorz, P.; Komaromi, I.; Martin, R. L.; Fox, D. J.; Keith, T.; Al-Laham, M. A.; Peng, C. Y.; Nanayakkara, A.; Challacombe, M.; Gill, P. M. W.; Johnson, B.; Chen, W.; Wong, M. W.; Gonzalez, C.; Pople, J. A. *Gaussian 03*, Revision C.02 ed.; Gaussian, Inc.: Pittsburgh, PA, 2004.
(17) Cances, E.; Mennucci, B.; Tomasi, J. *J. Chem. Phys.* **1997**, *107*, 3032–3041.
(18) Ma, C. S.; Kwok, W. M.; Chan, W. S.; Du, Y.; Kan, J. T. W.; Toy, P. H.; Phillips, D. L. *J. Am. Chem. Soc.* **2006**, *128*, 2558–2570.

JP808532N